Available online at www.sciencedirect.com
ScienceDirect
ELSEVIER
Ultramicroscopy 108 (2008) 339–345
ultramicroscopy
www.elsevier.com/locate/ultramic

Measurement of twofold astigmatism of probe-forming lens using low-order zone-axis ronchigram

Koji Kuramochi[a], Takashi Yamazaki[a,*], Yasutoshi Kotaka[b], Yoshio Kikuchi[b], Iwao Hashimoto[a], Kazuto Watanabe[c]

[a]*Department of Physics, Tokyo University of Science, 1-3 Kagurazaka/Shinjuku-ku, Tokyo 162-8601, Japan*
[b]*Fujitsu Laboratory Ltd., Kanagawa 243-0197, Japan*
[c]*Tokyo Metropolitan College of Industrial Technology, Tokyo 140-0011, Japan*

Received 18 October 2006; received in revised form 14 May 2007; accepted 25 May 2007

Abstract

By using a low-order zone-axis ronchigram of a crystalline sample, a simple method for measuring twofold astigmatism of a probe-forming lens is proposed. This method allows precise measurement of the value of astigmatism from only one experimental ronchigram.

PACS: 68.37.Lp; 61.14.Lj

Keywords: Ronchigram; STEM; Astigmatism; Lens aberration function

1. Introduction

Recently, in order to improve the spatial resolution of high-resolution transmission electron microscopy (TEM) and high-resolution scanning transmission electron microscopy (STEM), the development of a spherical aberration (C_s)-corrected electron microscope has been globally undertaken [1–6]. In the C_s-correction technique, the lens parameters of the electromagnetic lens need to be precisely measured. A power spectrum image of an amorphous film has been conventionally used to measure C_s coefficients [5–7]. However, for observing crystalline thin films, users must first tune the instrument on a test amorphous zone before moving to the observed area; they need to move back and forth between the amorphous and crystalline areas in order to re-tune the instrument when the microscope aberrations drift over time [8]. Here, it is difficult to measure the exact C_s coefficient of the observed area.

A ronchigram is an extreme case of a coherent convergent-beam electron diffraction (CBED) pattern that has been recorded using a large aperture or with the aperture removed entirely [9–14]. For a crystalline sample, the convergent beam disks overlap with each other and complicated patterns appear; these patterns are functions of several factors such as the crystal structure, probe position, sample thickness, defocus value, C_s and so on [14]. Recently, a precise method for measuring the C_s coefficient of a probe-forming lens was proposed that could be used even for an experimental ronchigram of a crystalline sample obtained at the low-order zone axis [15]. This method uses a characteristic fringe obtained from a three-wave interaction. However, it requires the elimination of the astigmatism of the probe-forming lens. Thus far, the method for measuring the twofold astigmatism of the probe-forming lens necessitated the use of an amorphous film. Recently, a method for measuring astigmatism using a low-order zone-axis ronchigram of a crystalline sample was proposed by Ramasse and Bleloch [8]. They improved the measurement accuracy by using an achromatic pattern obtained by integrating the through-focal series of the ronchigram;

*Corresponding author. Tel./fax: +81 3 3260 9787.
E-mail address: yamazaki@rs.kagu.tus.ac.jp (T. Yamazaki).

0304-3991/$ - see front matter
doi:10.1016/j.ultramic.2007.05.007

however, it was difficult to measure and/or adjust astigmatism in real time.

We believe that it is necessary to independently measure each lens parameter. Yamazaki et al. [15] measured the defocus values and the spherical aberration coefficient by using only a part dependent on each lens parameter. In this paper, since we could extract a part dependent on only astigmatism, we propose another simple and accurate method for measuring the twofold astigmatism using only one experimental low-order zone-axis ronchigram of a crystalline sample.

2. Methods

2.1. Experimental procedure

A $SrTiO_3$ (0 0 1) single crystal was used in the experiment. The samples were mechanically thinned and polished to a thickness of approximately 10 μm by using a dimple grinder. The final thinning was carefully performed by means of 4 keV Ar^+ ion milling at an angle of 4°. Since high-resolution images cannot be obtained when a large surface amorphous layer is present, ion milling was performed at the lowest possible angles at 1.7 keV in order to remove the amorphous films. Hence, it is considered that the statistical error introduced by any amorphous residue is not essential in the determination of astigmatism in an experimental ronchigram.

The experimental ronchigrams of $SrTiO_3$ (0 0 1) were obtained using JEM-2100F TEM/STEM. In this experiment, the aperture was entirely removed. This instrument was operated at 200 keV and equipped with a pole piece designed for $C_s = 0.5$ mm. The third-order C_s coefficient was determined as 0.476 mm using the method proposed by Yamazaki et al. [15]. The experimental ronchigram was recorded on a film because the entire ronchigram needed to have sufficient resolution in order to reduce errors. The recorded films were converted to two-dimensional digital data using an optical image scanner with a grey depth of 8 bits per pixel and a resolution of 2048 × 2048 pixels per image.

2.2. Measurement method of twofold astigmatism

A lens aberration function with twofold astigmatism can be expressed as

$$W(K_x, K_y) = \pi\lambda\left[\Delta f(K_x^2 + K_y^2) + \frac{\lambda^2}{2}C_s(K_x^2 + K_y^2)^2 + C_{1,2a}(K_x^2 - K_y^2) + 2C_{1,2b}K_xK_y\right], \quad (1)$$

where α, Δf and C_s denote the wavelength, defocus value and third-order C_s coefficient, respectively [16]. Further, $C_{1,2a}$ and $C_{1,2b}$ denote the values of twofold astigmatism; these values non-isotropically distort the lens aberration function to K_x and K_y, whereas C_s and Δf introduce an isotropic distortion. The distortion directions of each astigmatism parameter differ by 45°. In this study, the directions of K_x and K_y were set as [1 $\bar{1}$ 0] and [1 1 0], respectively. Thus, by setting up an axis of coordinates, the lens aberration functions form an ellipse whose major axis is set along the [1 0 0] direction based on the variation in the $C_{1,2a}$ value, and another major axis is set along the [1 1 0] direction based on the variation in the value of $C_{1,2b}$.

The calculated ronchigrams with and without astigmatism and the experimental images are shown in Figs. 1(a)–(c), respectively. In Fig. 1(b), $C_{1,2a} = C_{1,2b} = 80$ nm. According to the Bloch wave theorem, the dynamical simulation for a coherent CBED pattern was expanded to ronchigram simulation [15]. The defocus value that was roughly estimated from the experimental image was −800 nm. The simulated images shown in Figs. 1(a) and (b) were calculated for $\Delta f = -800$ nm. Each Fourier power spectrum (FPS) image is shown in Figs. 1(d)–(f), respectively. It should be noted that the image in Fig. 1(d) is symmetric. On the other hand, the FPS image of Fig. 1(b), as shown in Fig. 1(e), is asymmetric. The value of astigmatism can be measured from this asymmetry. In order to improve accuracy, the second Fourier power spectrum (SFPS) images obtained using the Fourier transform of each FPS image are used, as shown in Figs. 1(g)–(i) [17]. The pattern corresponds to a diffraction pattern of plane-wave incidence, and the positions of the bright spots do not change even if astigmatism is included.

A ronchigram, FPS image and an SFPS image which were calculated using three waves of $\mathbf{g} = 0\,0\,0$, $1\,\bar{1}\,0$ and $\bar{1}\,1\,0$ were used in order to investigate the image formation mechanism of an SFPS image, as displayed in Figs. 2(a)–(c), respectively. There are displacements of bright spots due to an astigmatism in the FPS image. Furthermore, bright spots which are not affected by lens parameters were observed in the SFPS image. At this stage, the ronchigram, FPS image and SFPS image were calculated by using only the lens aberration function as shown in Figs. 2(d)–(f), respectively. The characteristics of Figs. 2(a)–(c) and Figs. 2(d)–(f) are similar. Therefore, it has been found that the characteristics of the FPS and SFPS images are mainly dominated by a lens aberration function. Figs. 2(g)–(o) show ronchigrams, FPS and SFPS images which were calculated by considering the astigmatism, defocus and the spherical aberration coefficient. The bright spots in the FPS image are displaced only along the direction of astigmatism, and the effect of defocus produces the bright spots in the FPS image along the [1 0 0] axis. Since the bright spots in the FPS image can be explained by simultaneously considering these two effects, we can measure the value of astigmatism by measuring the displacement of the bright spots in the FPS image. However, it should be noted that there are no clear bright spots in the SFPS images which can be calculated using only astigmatism or defocus. On the other hand, in the ronchigram simulated using only the spherical aberration coefficient, bright spots appear in the SFPS image as shown

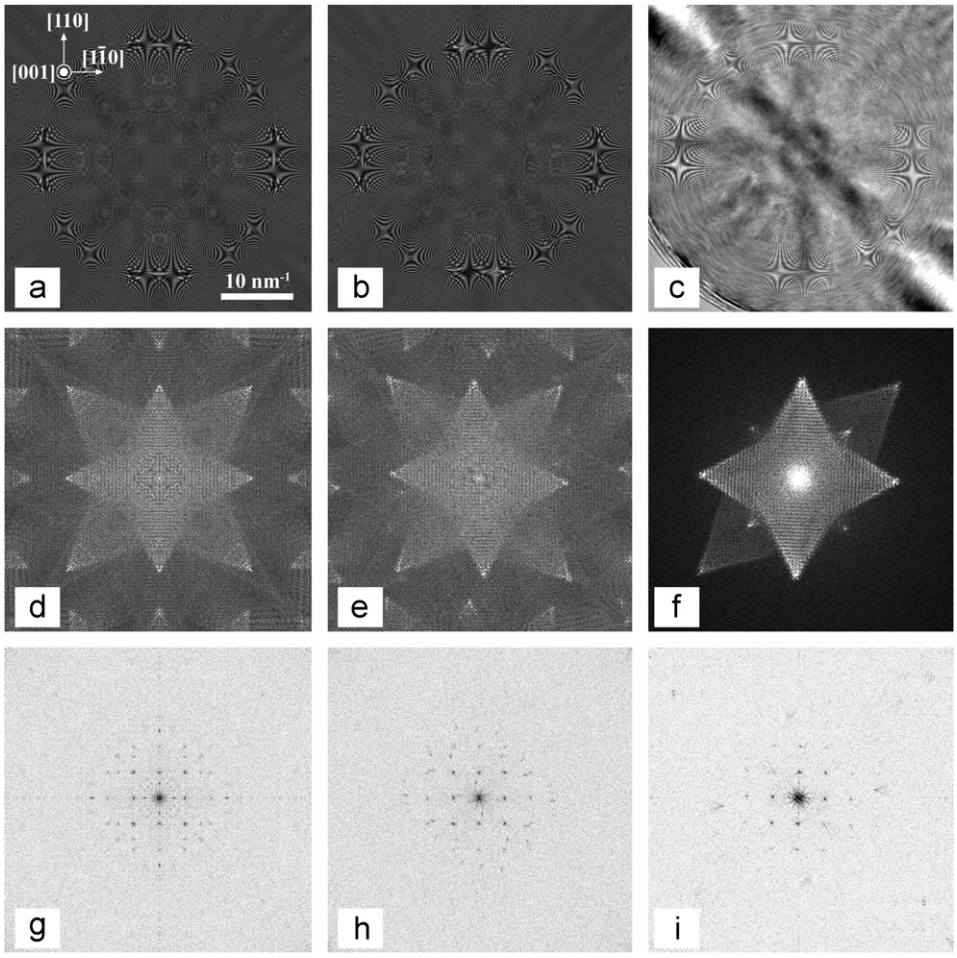

Fig. 1. (a) Simulated ronchigram of [0 0 1]-orientated $SrTiO_3$ with no astigmatism. (b) Simulated ronchigram with astigmatism. (c) Experimental ronchigram. (d–f) Corresponding FPS and (g–i) SFPS images.

in Fig. 2(o). However, there are no clear bright spots as in the FPS image. Based on this fact, we ascertain that bright spots in an SFPS image are mainly described by a spherical aberration coefficient. Furthermore, the characteristics of the FPS images, shown in Figs. 2(k) and (n), indicate that the lens parameters exhibiting the symmetrical distortion do not affect the value of astigmatism measured by the present method.

The lens aberration function considering only the spherical aberration coefficient is given by

$$\begin{aligned} W(K_x+g,K_y) &= \frac{\pi\lambda^3 C_s}{2}[(K_x+g)^2+K_y^2]^2 \\ &= \frac{\pi\lambda^3 C_s}{2}[(K_x+K_y)^2+4K_x^3g+6K_x^2g^2 \\ &\quad +4K_xg^2+g^4+4K_xK_y^2g+2K_y^2g^2]. \end{aligned} \quad (2)$$

The terms independent of the K_y-component give the value only along the R_x-axis in an FPS image. Therefore, these terms do not influence the appearance of bright spots in the SFPS image. The simulated results of the ronchigram, FPS image and SFPS image which are calculated only by the lens aberration function including the K_y-component are shown in Figs. 2(p)–(r), respectively. The characteristic of the SFPS image shown in Fig. 2(c) is reproduced well in Fig. 2(r). The ronchigram obtained by the restricted lens aberration function is expressed by

$$\begin{aligned} I(K_x,K_y) &= \left|\sum_g \exp\left\{\mathrm{i}\frac{\pi\lambda^3 C_s}{2}[(K_x+K_y)^2\right.\right. \\ &\quad \left.\left.+4K_xK_y^2g+2K_y^2g^2]\right\}\right|^2 \\ &= 3+2\cos(\pi\lambda^3 C_sK_y^2g^2) \\ &\quad +4\cos(2\pi\lambda^3 C_sK_xK_y^2g)\cos(\pi\lambda^3 C_sK_y^2g^2). \end{aligned} \quad (3)$$

The values of the terms depending on K_y and the constant value are negligible for the same reasons as mentioned above. Therefore, the FPS image is computed by

$$\begin{aligned} \Phi(R_x,R_y) &= \mathrm{FT}[4\cos(2\pi\lambda^3 C_sK_xK_y^2g)\cos(\pi\lambda^3 C_sK_y^2g^2)] \\ &= 4\int \mathrm{d}K_y\cos(\pi\lambda^3 C_sK_y^2g^2)\exp(2\pi\mathrm{i}K_yR_y) \\ &\quad \times\int \cos(2\pi\lambda^3 C_sK_xK_y^2g)\exp(2\pi\mathrm{i}K_xR_x)\,\mathrm{d}K_x \end{aligned}$$

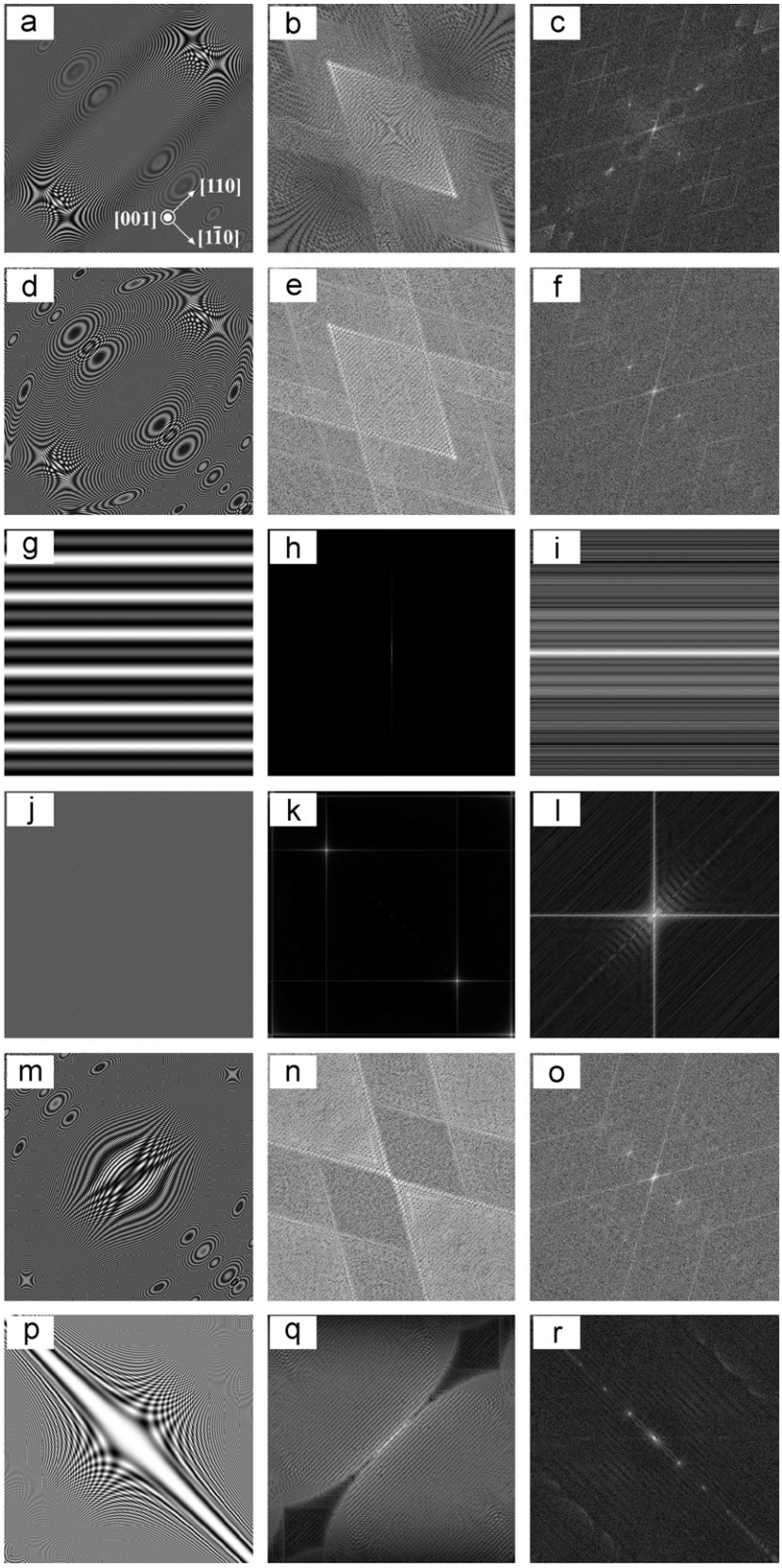

Fig. 2. (a) Simulated ronchigram of [0 0 1]-orientated $SrTiO_3$ under three beams condition; (b) and (c) its corresponding FPS and SFPS images. (d)–(f) Ronchigram, FPS and SFPS images calculated by using only lens aberration function. (g)–(i) Ronchigram, FPS and SFPS images calculated using lens aberration function including only the effect of defocus. (j)–(l) Effect of an astigmatism. (m)–(o) Effect of a spherical aberration coefficient, respectively. (p)–(r) Ronchigram, FPS and SFPS images calculated by restricted lens aberration function expressed by Eq. (3). In order to ease-to-seeing a change of bright spots of FPS and SFPS images, the horizontal axis of outputted figures is turned 45° against K_x-axis.

$$= 4 \int \cos(\pi\lambda^3 C_s K_y^2 g^2) \exp(2\pi i K_y R_y) \times [\delta(\lambda^3 C_s K_y^2 g + R_x) + \delta(-\lambda^3 C_s K_y^2 g + R_x)]\, dK_y = 4 \cos(\pi |R_x| g) \exp\left[2\pi i R_y \left(\frac{R_x}{\lambda^3 C_s g}\right)^{1/2}\right]. \quad (4)$$

Hence, the intensity of the FPS image is given by

$$|\Phi(R_x, R_y)|^2 = 16\cos^2(\pi |R_x| g) = 8\cos(2\pi |R_x| g) + 8. \quad (5)$$

It should be noted that the intensity has a cosine function described by a period of $2\pi g$. The bright spots in an SFPS image are mainly described by this function. Therefore, these images can be used as the standard axis in reciprocal space. As a result, we can precisely measure astigmatism from only one experimental ronchigram.

Fig. 3(a) shows the image of Fig. 1(b) enlarged in the central region. The corresponding FPS image is shown in Fig. 3(b). Each bright spot in the FPS image coincides with each Bragg reflection that appears in the diffraction pattern, although the dimensions of the FPS image are in real space. In this figure, $\Delta R'_{1,2a}$ and $\Delta R'_{1,2b}$ are defined as the parameters that indicate each displacement from the symmetry of a crystal. The R'_x-axis and R'_y-axis indicating the symmetry of a crystal are determined from the SFPS image. On the basis of a theoretical analysis, the relationship between the displacement and the value of astigmatism is given by

$$C_{1,2a} = \frac{1}{\lambda g_a} \Delta R'_{1,2a} \quad (6)$$

and

$$C_{1,2b} = \frac{1}{\lambda g_b} \Delta R'_{1,2b}, \quad (7)$$

where g_a and g_b are reciprocal lattice vectors corresponding to bright spots in the FPS image which are used to measure $C_{1,2a}$ and $C_{1,2b}$, respectively. The algebraic steps for deriving Eqs. (6) and (7) are described in Appendix A.

It appears nevertheless that Eqs. (6) and (7) are only valid in a very limited number of cases. In other words, the example chosen here is very convenient: the angle between the $1\,\bar{1}\,0$ and the $0\,0\,2$ reflections for a cubic crystal in [0 0 1] orientation is precisely 45°, which happens to be the correct symmetry for astigmatism. However, we suggest that astigmatism in a crystal which did not have the correct symmetry for astigmatism can be measured by performing appropriate coordinate transformation. The details of the method are shown in Appendix B. By this expansion, the measurement of astigmatism is possible in any kind of crystal although the equation becomes slightly complicated.

In Fig. 3(b), the measured values of $\Delta R'_{1,2a}$ and $\Delta R'_{1,2b}$ are 0.73 and 1.00 nm, respectively. Astigmatism is determined by substituting these values in Eqs. (6) and (7). In Fig. 3(b), the bright spots are used for measuring astigmatism corresponding to the $(1\,\bar{1}\,0)$ and $(2\,0\,0)$ reflections. The relationships of Eqs. (6) and (7) with each reflection are plotted in Fig. 3(c). The measured values of astigmatism are 80.3 ± 1.9 and 77.8 ± 1.3 nm. This error is attributed to the detection resolution of the FPS image. In the present case, error in the detection of peak search was estimated as 1 pixel. From Eqs. (6) and (7), a change of $\Delta R'_{1,2a}$ and $\Delta R'_{1,2b}$ increases against a change of an astigmatism by increasing g_a and g_b which are used to measurement. Therefore, high angle reflection is sensitive to a change in astigmatism; hence, it is used to improve the accuracy. In the experimental image, a relative error due to slightly residual higher-order astigmatism, such as coma and threefold astigmatism, is added to the detected error. This relative error is estimated from the statistical treatment of the measured results in some equivalent bright spots.

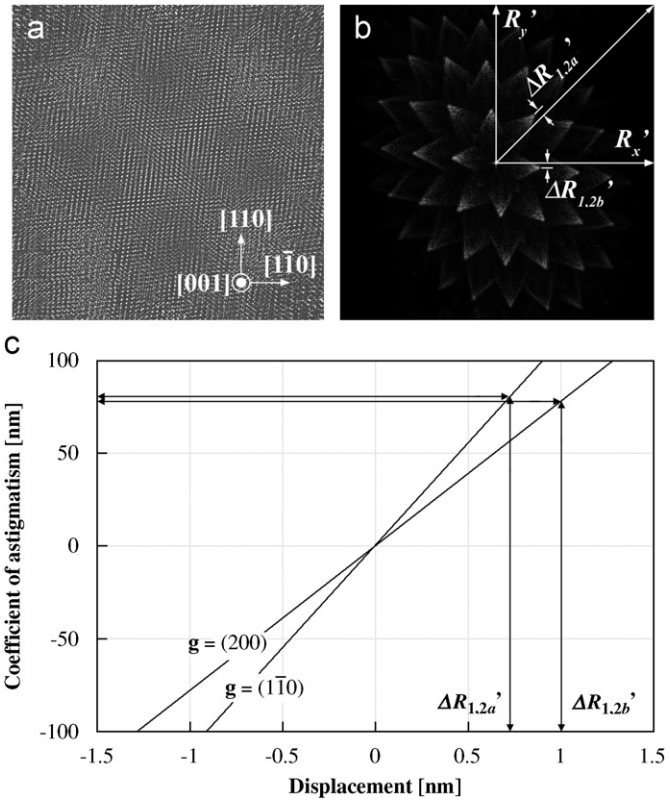

Fig. 3. (a) Magnified ronchigram of the framed area in Fig. 1(b). (b) FPS image of (a). (c) Relationships of the astigmatism and displacement of bright spots in FPS image. $\Delta R'_{1,2a}$ and $\Delta R'_{1,2b}$ used to measure astigmatism are shown together.

3. Results

In order to confirm the validity of the present method, the values of astigmatism of the experimental image, which were obtained by rotating the multifunctional knobs, were quantitatively measured. The ronchigrams recorded for three different values of astigmatism are shown in Figs. 4(a)–(c). The experimental conditions of these images were based on the lens current value at

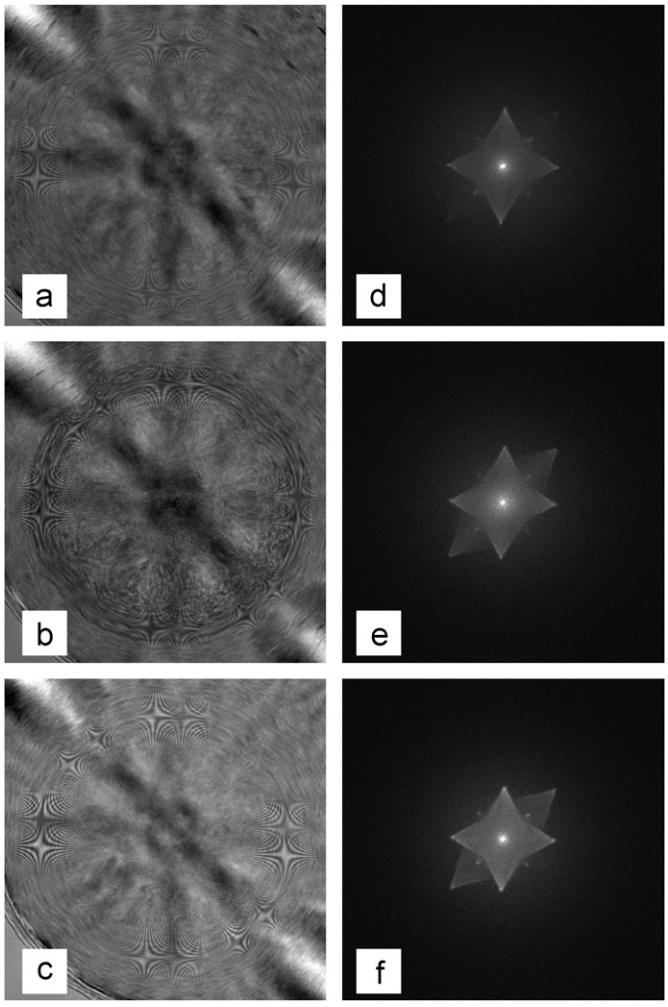

Fig. 4. (a)–(c) Experimental ronchigrams recorded for three types of astigmatism. (d)–(f) The corresponding FPS images.

Table 1
Measured results for three types of experimental images

	Pattern A	Pattern B	Pattern C
$C_{1,2a}$ [nm]	10.5 ± 2.9	30.9 ± 3.7	4.0 ± 2.7
$C_{1,2b}$ [nm]	-6.8 ± 1.9	-0.5 ± 2.7	4.8 ± 1.7

which pattern A was recorded. Patterns B and C were recorded by rotating the x-knob and y-knob of the multifunctional knobs from the base condition, respectively. The extent of the step-wise change in the lens current value due to each multifunctional knob was 0.5 mA. The FPS images corresponding to each image are shown in Figs. 4(d)–(f). The measured results of the astigmatism values for each image are listed in Table 1. The influence of different orientations—achieved by changing each current knob—on astigmatism was measured. Furthermore, the astigmatism was measured by the present method, and we discussed its influence on the atomic-resolution STEM in detail [18].

4. Summary

By using a low-order zone-axis ronchigram, a measurement method for twofold astigmatism of a probe-forming lens is proposed. By using the SFPS image of the ronchigram as the standard axis in reciprocal space, the accuracy is drastically improved as compared to the measurement without the SFPS image. If a STEM is equipped with a CCD camera with a resolution equivalent to that of the present measurement, it may be possible to achieve real-time adjustment.

Appendix A

The simulation method of a ronchigram was based on the simulation method of a coherent CBED pattern. In order to simplify the algebraic steps for deriving Eqs. (6) and (7), a three-wave calculation with $\pm\mathbf{g}$ reflections along the K_x direction was considered, and the C_s was set to be 0. In this case, the ronchigram intensity can be given by following equation:

$$\begin{aligned} I(\mathbf{K}_f, t) &= \left| \sum_g T_g(\mathbf{K}_f - \mathbf{g}) \exp[\mathrm{i} W(\mathbf{K}_f - \mathbf{g})] \right|^2 \\ &= T_0(\mathbf{K}_f) T_0^*(\mathbf{K}_f) + T_g(\mathbf{K}_f - \mathbf{g}) T_g^*(\mathbf{K}_f - \mathbf{g}) \\ &\quad + T_{-g}(\mathbf{K}_f + \mathbf{g}) T_{-g}^*(\mathbf{K}_f + \mathbf{g}) \\ &\quad + T_0(\mathbf{K}_f) T_g^*(\mathbf{K}_f - \mathbf{g}) \exp\{\mathrm{i}[W(\mathbf{K}_f) - W(\mathbf{K}_f - \mathbf{g})]\} \\ &\quad + T_0(\mathbf{K}_f) T_{-g}^*(\mathbf{K}_f + \mathbf{g}) \exp\{\mathrm{i}[W(\mathbf{K}_f) - W(\mathbf{K}_f + \mathbf{g})]\} \\ &\quad + T_g(\mathbf{K}_f - \mathbf{g}) T_0^*(\mathbf{K}_f) \exp\{\mathrm{i}[W(\mathbf{K}_f - \mathbf{g}) - W(\mathbf{K}_f)]\} \\ &\quad + T_g(\mathbf{K}_f - \mathbf{g}) T_{-g}^*(\mathbf{K}_f + \mathbf{g}) \exp\{\mathrm{i}[W(\mathbf{K}_f - \mathbf{g}) \\ &\quad - W(\mathbf{K}_f + \mathbf{g})]\} + T_{-g}(\mathbf{K}_f + \mathbf{g}) T_0^*(\mathbf{K}_f) \\ &\quad \times \exp\{\mathrm{i}[W(\mathbf{K}_f + \mathbf{g}) - W(\mathbf{K}_f)]\} \\ &\quad + T_{-g}(\mathbf{K}_f + \mathbf{g}) T_g^*(\mathbf{K}_f - \mathbf{g}) \\ &\quad \times \exp\{\mathrm{i}[W(\mathbf{K}_f + \mathbf{g}) - W(\mathbf{K}_f - \mathbf{g})]\}, \end{aligned} \tag{8}$$

where $\mathbf{K}_f = (K_x, K_y)$ and T_g is the transmission coefficient of the $\mathbf{g}$ reflection. The first three terms are independent of the lens aberration function. The change in these terms to $\mathbf{K}_f$ is minimal when compared with the change in the lens aberration function. Therefore, since these terms hardly affect the contrast of an FPS image, it has been found that the coupling terms of the lens aberration function mainly contribute to the FPS image. The coupling terms of the lens aberration function are given by

$$\begin{aligned} W(\mathbf{K}_f) - W(\mathbf{K}_f - \mathbf{g}) &= W(K_x, K_y) - W(K_x - g, K_y) \\ &= 2\pi\lambda\Delta f K_x g - \pi\lambda\Delta f g^2 + 2\pi\lambda C_{1,2a} K_x g \\ &\quad - \pi\lambda C_{1,2a} g^2 + 2\pi\lambda C_{1,2b} g K_y \\ &\equiv \Omega(K_x) + 2\pi\lambda C_{1,2b} g K_y. \end{aligned} \tag{9}$$

In this equation, only one term that depends on K_y remains. The results of the Fourier transform with respect

to $\mathbf{K}_f$ of the coupling term of the lens aberration function are given by

$$\begin{aligned}\tilde{I}(\mathbf{R}') &= \mathrm{FT}[\exp\{\mathrm{i}[W(\mathbf{K}_f) - W(\mathbf{K}_f - \mathbf{g})]\}] \\ &= \int \exp\{\mathrm{i}[\Omega(K_x) + 2\pi\lambda C_{1,2b} g K_y]\} \exp(2\pi\mathrm{i}\mathbf{K}_f \cdot \mathbf{R}')\,\mathrm{d}\mathbf{K}_f \\ &= \left[\int \exp[\mathrm{i}\Omega(K_x)] \exp(2\pi\mathrm{i}K_x x')\,\mathrm{d}K_x\right] \\ &\quad \times \left[\int \exp[\mathrm{i}(2\pi\lambda C_{1,2b} g + 2\pi y')K_y]\,\mathrm{d}K_y\right] \\ &= \left[\int \exp[\mathrm{i}\Omega(K_x)] \exp(2\pi\mathrm{i}K_x x')\,\mathrm{d}K_x\right] \\ &\quad \times \delta(2\pi\lambda C_{1,2b} g + 2\pi y'). \end{aligned} \tag{10}$$

In this case, we focus our attention on the term that depends on y'. As a result, since a change in a direction perpendicular to that of systematic reflection is set to y', the relationship between the coefficient of astigmatism and y' is expressed by the following equation:

$$y' = -\lambda g C_{1,2b}.$$

Furthermore, it is also important that displacement in a direction perpendicular to that of systematic reflection is dependent only on one astigmatism parameter. Therefore, based on the deviation from the direction of systematic reflection, one independent astigmatism parameter can be determined, and the slope is proportional to the **g** reflection and wavelength. In the case of a limited C_s coefficient, its influence is considered as the error function. The error function forms a triangle with one of its vertices at the position of the delta function shown in Eq. (10). Fortunately, since the limited C_s coefficient did not influence the function in Eq. (10), the value of the C_s coefficient did not affect the present measurement.

Appendix B

Here, two reciprocal spots $\mathbf{g}_1$ and $\mathbf{g}_2$ which form an angle of θ with each other and two rectangular coordinates named U-system and V-system have been introduced. The x-axis in the U-system is then orientated to $\mathbf{g}_1$, and the x-axis in V-system to $\mathbf{g}_2$. In this case, these two systems have the following relation:

$$\begin{pmatrix} V_x \\ V_y \end{pmatrix} = \begin{pmatrix} \cos\theta & \sin\theta \\ -\sin\theta & \cos\theta \end{pmatrix} \cdot \begin{pmatrix} U_x \\ U_y \end{pmatrix}, \tag{11}$$

where U_x and U_y are the x and y components of the U-system and V_x and V_y of the V-system. Then, the lens parameters of twofold astigmatism in the U-system ($C_{1,2a}$ and $C_{1,2b}$) and in the V-system ($C'_{1,2a}$and $C'_{1,2b}$) are obtained as follows:

$$\begin{aligned} &C_{1,2a}(U_x^2 - U_y^2) + 2C_{1,2b}U_xU_y \\ &\quad = C'_{1,2a}(V_x^2 - V_y^2) + 2C'_{1,2b}V_xV_y \\ &\quad = (C'_{1,2a}\cos 2\theta - C'_{1,2b}\sin 2\theta)(U_x^2 - U_y^2) \\ &\qquad + 2(C'_{1,2a}\sin 2\theta + C'_{1,2b}\cos 2\theta)U_xU_y. \end{aligned} \tag{12}$$

Therefore, the relationship between ($C_{1,2a}$ and $C_{1,2b}$) and ($C'_{1,2a}$and $C'_{1,2b}$) is described by

$$\begin{pmatrix} C_{1,2a} \\ C_{1,2b} \end{pmatrix} = \begin{pmatrix} \cos 2\theta & -\sin 2\theta \\ \sin 2\theta & \cos 2\theta \end{pmatrix} \cdot \begin{pmatrix} C'_{1,2a} \\ C'_{1,2b} \end{pmatrix}, \tag{13}$$

$C_{1,2b}$ and $C'_{1,2b}$ can be measured by our method; hence, $C_{1,2a}$ and $C'_{1,2a}$ can be calculated from Eq. (13).

References

[1] M. Haider, S. Uhlemann, E. Schwan, H. Rose, B. Kabius, K. Urban, Nature 392 (1998) 768.
[2] P.E. Batson, N. Dellby, O.L. Krivanek, Nature 418 (2002) 617.
[3] J.L. Hutchison, J.M. Titchmarsch, D.J.H. Cockayne, G. Möbus, C.J.D. Hetherington, R.C. Doole, F. Hosokawa, P. Hartel, M. Haider, Microsc. Anal. 8 (Suppl. 2) (2002) 10.
[4] H. Sawada, T. Tomita, M. Naruse, T. Honda, P. Hambridge, P. Hartel, M. Haider, C. Hetherington, R. Doole, A. Kirk, J. Hutchison, J. Titchmarsh, D.J.H. Cockayne, J. Electron Microsc. 54 (2) (2005) 119.
[5] N. Dellby, O.L. Krivanek, P.D. Nellist, P.E. Batson, A.R. Lupini, J. Electron Microsc. 50 (3) (2001) 177.
[6] F. Hosokawa, T. Tomita, M. Naruse, T. Honda, P. Hartel, M. Haider, J. Electron Microsc. 52 (1) (2003) 3.
[7] K. Wong, E. Kirkland, P. Xu, R. Loane, J. Silcox, Ultramicroscopy 40 (1992) 139.
[8] Q.M. Ramasse, A.L. Bleloch, Ultramicroscopy 106 (2005) 37.
[9] J.A. Lin, J.M. Cowley, Ultramicroscopy 19 (1986) 179.
[10] J.A. Lin, J.M. Cowley, Ultramicroscopy 19 (1986) 31.
[11] J.M. Cowley, J. Electron Microsc. Tech. 3 (1986) 25.
[12] E.M. James, N.D. Browning, A.W. Nicholls, M. Kawasaki, Y. Xin, S. Stemmer, J. Electron Microsc. 47 (6) (1998) 561.
[13] V. Ronchi, Appl. Opt. 3 (1964) 437.
[14] J.C.H. Spence, J.M. Zuo, Electron Microdiffraction, Plenum Press, New York, 1992.
[15] T. Yamazaki, Y. Kotaka, Y. Kikuchi, K. Watanabe, Ultramicroscopy 106 (2006) 153.
[16] O.L. Krivanek, N. Delly, A.R. Lupini, Ultramicroscopy 78 (1999) 1.
[17] Y. Kotaka, T. Yamazaki, K. Watanabe, N. Nakanishi, Patent 2005-298799, 2006 (in Japanese).
[18] T. Yamazaki, K. Watanabe, K. Kuramochi, Y. Kotaka, Y. Kikuchi, I. Hashimoto, in: Proceedings of the 16th International Microscopy Congress, 2006, p. 624.